



September 7. - 9.9.2009

Cheb, Czech Republic

# INFINITE BOUNDARY ELEMENT APPLICATION IN OPTICAL MAMMOGRAPHY

MACIEJ PANCZYK, M.SC. ENG.  
PROF. JAN SIKORA, D.SC. PH.D.

**Abstract:** Early detection or screening examination of breast cancer can be done using Optical Tomography or Electrical Impedance Tomography. Using Boundary Element Method for forward problem solution we can not make measurements or precisely define boundary conditions on the surface between breast and chest. A simple solution is to extend the mesh outside the region of interest and to truncate it in some distance from the investigated human breast. Wrong boundary conditions or improper placement of such artificial boundary can introduce an unknown error if the truncation occurs too near. On the other hand excessive mesh increases number of boundary elements and decreases the computational efficiency especially annoying while calculating inverse problem solution. Some discussion on a few simple models of the breast will be presented. Last model contains infinite boundary elements. Implementation of such elements can reduce the mesh and avoid the problem of setting incorrect boundary conditions by creating an open boundary model.

**Key words:** Boundary Element Method, Infinite Elements, Optical Tomography

## INTRODUCTION

Electrical Impedance Tomography and Optical Tomography can use Boundary Element Method (BEM) for forward problem solution [1,6,7,8]. On the area of human female breast cancers investigations it is only possible to make measurements on the skin. The boundary surface between breast and chest remains unavailable for detectors placement. It is also difficult to set precise boundary condition on that surface. A typical simple BEM solution is to extend the boundary element mesh outside the zone of interest and to truncate it at a large distance away so that the new boundary does not influence the results. Such solution generates a large number of additional boundary elements and in case that truncation occurs too near can introduce an unknown error. A more effective method is to incorporate infinite boundary elements [3,4] into conventional BEM analysis. Infinite elements [5] usage was at first adopted in wave propagation and geotechnical problems. In our case it is to estimate the differences between models and to consider if it is worth to extend analysed area or to implement infinite elements into breast geometry.

## 1 MODELS DESCRIPTION

Four simple theoretical models of human breast were investigated. For all models one placement of the light

source was presented - located near the bottom of the hemisphere model. First model presented on fig. 2 corresponds to the pure hemisphere. Second model was extended by adding a cylinder in the bottom (fig. 3). The intention of it was to avoid possible errors on the bottom of the hemisphere. The next one develop that idea by adding the cylinder with identical height but bigger diameter (fig. 4). It is to eliminate the errors near the basis circumference. All models were constructed from 1536 second order eight nodes quadrilateral boundary elements and 4610 nodes. Half of the elements covers hemisphere.

Governing equation for the problem is diffusion approximation of the transport equation (Helmholtz - assuming scattering and absorption are homogeneous):

$$\nabla^2 \Phi(\mathbf{r}, \omega) - k^2 \Phi(\mathbf{r}, \omega) = -\frac{q_0(\mathbf{r}, \omega)}{D}, \quad \forall \mathbf{r} \in \Omega/\Gamma, \quad (1)$$

Where  $\Phi$  stands for the photon density, wave number

$$k = \sqrt{\frac{\mu_a}{D} - j \frac{\omega}{cD}} \quad \text{and} \quad \text{diffusion coefficient}$$

$D = [3(\mu_a + \mu'_s)]^{-1}$ ,  $\mu_a$  is an absorbing and  $\mu'_s$  is reduced scattering coefficient [1]  $\mu'_s = \mu_s(1-g)$  [ $\text{cm}^{-1}$ ],  $g$  is the average cosine of the scattering angle and speed of light

$c(\mathbf{r}) = c_0/\nu(\mathbf{r})$ , where  $\nu(\mathbf{r})$  is the refractive index and  $c_0$  the speed of light in a vacuum,  $q_0$  is a source of light. There are Robin boundary conditions on the surfaces with different coefficients for breast tissue and for skeletal muscles on the basis [1,2,7] imposed:

$$\Phi(\mathbf{r}, \omega) + 2\alpha D \frac{\partial \Phi(\mathbf{r}, \omega)}{\partial n} = 0, \quad \forall \mathbf{r} \in \Gamma, \quad (2)$$

where  $\alpha$  models the refractive index difference at the boundary  $\Gamma$  [8].

Last open boundary model consists from 768 standard boundary elements and 64 infinite mapped elements based on eight nodes second order quadrilateral boundary elements [5,3,4]. The number of nodes is reduced to 2433 nodes in that case (fig. 5).

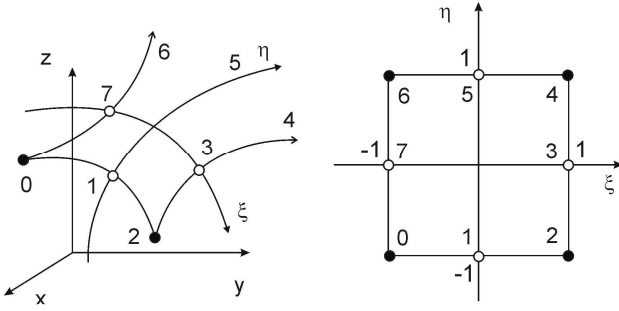


Figure 1. Five node mapped infinite boundary element based on 8 node quadrilateral isoparametric boundary element.

Serendipity infinite mapping functions [5]:

$$\begin{aligned} M_1 &= \frac{2}{1-\eta} (1-\xi^2), \\ M_3 &= \frac{1+\eta}{1-\eta} \frac{1}{2} (1-\xi), \quad M_7 = \frac{1+\eta}{1-\eta} (1+\xi^2), \\ M_2 &= \frac{-1-\eta+\eta\xi+\eta^2}{1-\eta}, \quad M_0 = \frac{-1-\eta-\eta\xi+\xi^2}{1-\eta}. \end{aligned} \quad (3)$$

were used for element transformation like presented on figure 1. These mapping functions (3) are used only for geometry transformation, not for physical quantities. Geometry transformation can be described by:

$$\begin{aligned} x(\xi, \eta) &= \sum_{n=0}^7 x_n N_n, & x(\xi, \eta) &= \sum_{m=0,1,2,3,7} x_m M_m, \\ y(\xi, \eta) &= \sum_{n=0}^7 y_n N_n, & y(\xi, \eta) &= \sum_{m=0,1,2,3,7} y_m M_m, \\ z(\xi, \eta) &= \sum_{n=0}^7 z_n N_n, & z(\xi, \eta) &= \sum_{m=0,1,2,3,7} z_m M_m, \end{aligned} \quad (4)$$

where  $n, m$  are number of standard and infinite elements respectively,  $N$  are basis interpolation functions [6] and  $M_m$  are mapping functions for infinite elements.

In equation (4) left column represents transformation for standard boundary elements and right column for infinite boundary elements.

Relevant boundary integral equation for surfaces covered by standard and infinite elements can be written as:

$$\begin{aligned} C(\mathbf{r})\Phi(\mathbf{r}) + \int_{\Gamma} \frac{\partial G(\mathbf{r}-\mathbf{r}', \omega)}{\partial n} \Phi(\mathbf{r}') d\Gamma + \\ + \int_{\Gamma_{\infty}} \frac{\partial G(\mathbf{r}-\mathbf{r}', \omega)}{\partial n} \Phi(\mathbf{r}') d\Gamma_{\infty} = \int_{\Gamma} G(\mathbf{r}-\mathbf{r}', \omega) \frac{\partial \Phi(\mathbf{r}')}{\partial n} d\Gamma + (5) \\ + \int_{\Gamma_{\infty}} G(\mathbf{r}-\mathbf{r}', \omega) \frac{\partial \Phi(\mathbf{r}')}{\partial n} d\Gamma_{\infty} - \sum_{S=0}^{n_S-1} Q_S G(\mathbf{r}_S - \mathbf{r}, \omega) \end{aligned}$$

where  $Q_S$  is the magnitude of the concentrated source ( $q_0 = Q_S \delta(\mathbf{r}_S)$ ) and  $n_S$  is a number of these sources.

For the diffusion equation the fundamental solution is:

$$G(\mathbf{r}-\mathbf{r}', \omega) = \frac{1}{4\pi|\mathbf{r}-\mathbf{r}'|} e^{-k|\mathbf{r}-\mathbf{r}'|} \quad (6)$$

For isoparametric quadratic quadrilateral element either standard or infinite we will have:

$$\Phi(\mathbf{r}) = \sum_{n=0}^7 \Phi_n N_n(\mathbf{r}), \quad \frac{\partial \Phi(\mathbf{r})}{\partial n} = \sum_{n=0}^7 \frac{\partial \Phi_n}{\partial n} N_n(\mathbf{r}) \quad (7)$$

It is to remember that for infinite mapped elements only nodes 0,1,2,3,7 are calculated.

The normal derivative of the Green function in a direction  $\mathbf{n}$  can be written:

$$\mathbf{n} \cdot \nabla G = \mathbf{n} \cdot \frac{\mathbf{r}-\mathbf{r}'}{|\mathbf{r}-\mathbf{r}'|} \left( \frac{-1}{4\pi|\mathbf{r}-\mathbf{r}'|^2} - \frac{k}{4\pi|\mathbf{r}-\mathbf{r}'|} \right) e^{-k|\mathbf{r}-\mathbf{r}'|} \quad (8)$$

Kernels required for normal derivative calculation can be written as:

$$\begin{aligned} \frac{\partial G}{\partial x} &= \frac{-k - \frac{1}{|\mathbf{r}-\mathbf{r}'|}}{4\pi|\mathbf{r}-\mathbf{r}'|} (x-x') e^{-k|\mathbf{r}-\mathbf{r}'|} \\ \frac{\partial G}{\partial y} &= \frac{-k - \frac{1}{|\mathbf{r}-\mathbf{r}'|}}{4\pi|\mathbf{r}-\mathbf{r}'|} (y-y') e^{-k|\mathbf{r}-\mathbf{r}'|} \\ \frac{\partial G}{\partial z} &= \frac{-k - \frac{1}{|\mathbf{r}-\mathbf{r}'|}}{4\pi|\mathbf{r}-\mathbf{r}'|} (z-z') e^{-k|\mathbf{r}-\mathbf{r}'|} \end{aligned} \quad (9)$$

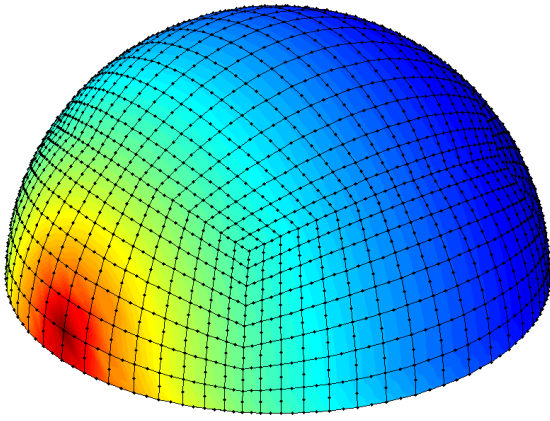


Figure 2. Base model of the breast – hemisphere.

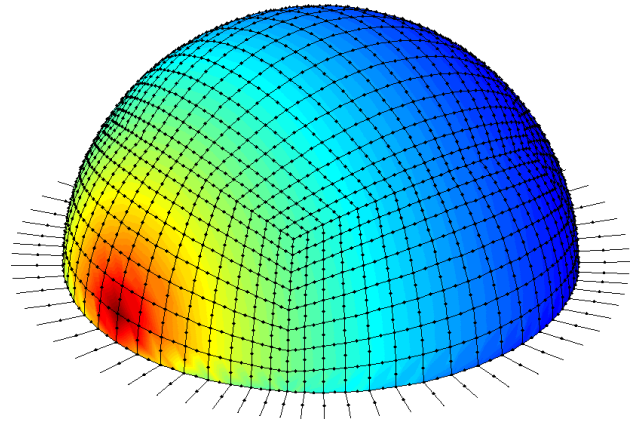


Figure 5. Open boundary hemisphere breast model with infinite boundary elements on the bottom.

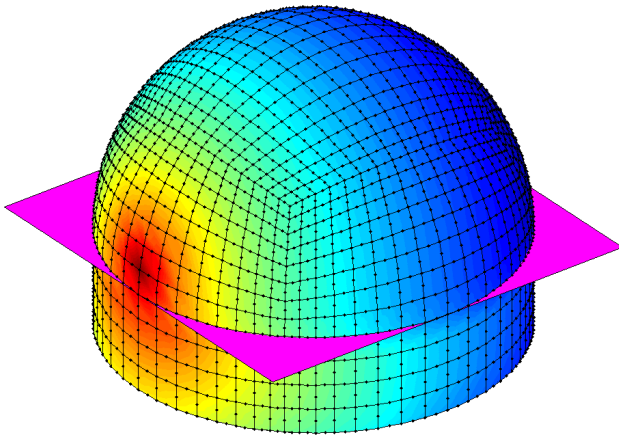


Figure 3. Extended model with additional part of chest, hemisphere with cylinder on the bottom.

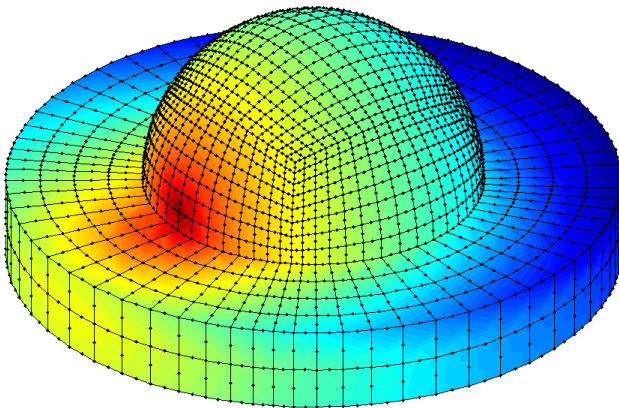


Figure 4. Extended model with additional part of chest, hemisphere with wider cylinder on the bottom.

## 2 RESULTS

Values of  $\partial\Phi/\partial n$  module and phase of the light at hemisphere circumference cross-section for  $y=0$  are presented on figure 6 and figure 7 respectively. To estimate the solution differences models with extended bottom part - figure 3, 4 and 5 were compared to basic hemisphere one - figure 2 and presented on figures 8 and 9. The solution has worst smoothness while decreasing mesh density and significant growth of calculation time without special accuracy improvement while increasing number of elements. Generally three extended models offers similar results, remarkably different then achieved while using the simplest hemisphere one. It is to notice that there is a logarithmic scale on  $\partial\Phi/\partial n$  module graph 6. The medium approximation differences for module is about 30% and for phase oscillates mainly about 3%. Near the hemisphere basis differences are grater and for module reaches even 130% and for phase exceeds 25%.

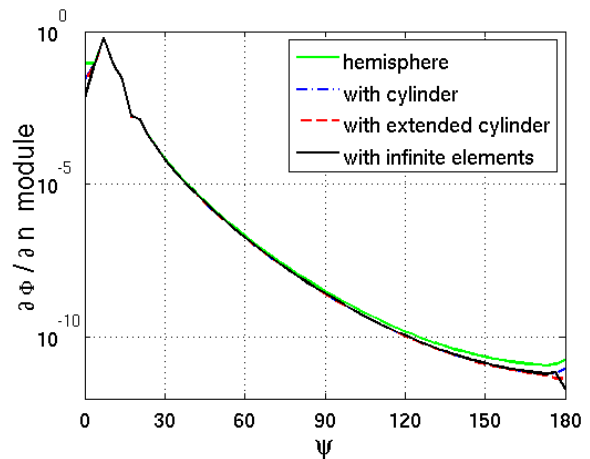


Figure 6. Results comparison for  $\partial\Phi/\partial n$  module.

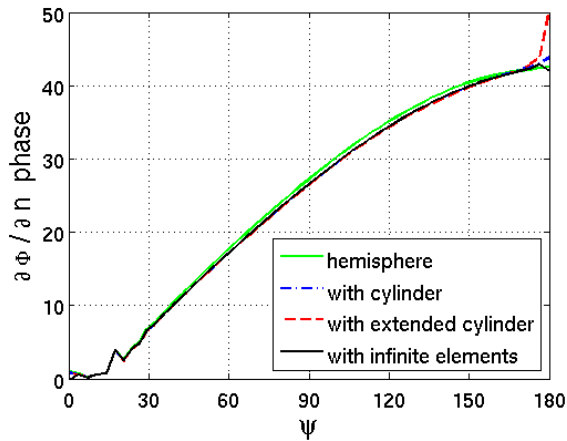


Figure 7. Results comparison for  $\partial\Phi/\partial n$  phase.

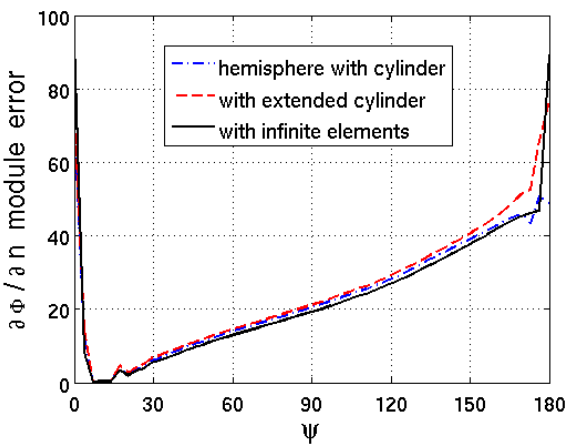


Figure 8. Solution differences for  $\partial\Phi/\partial n$  module compared to hemisphere model.

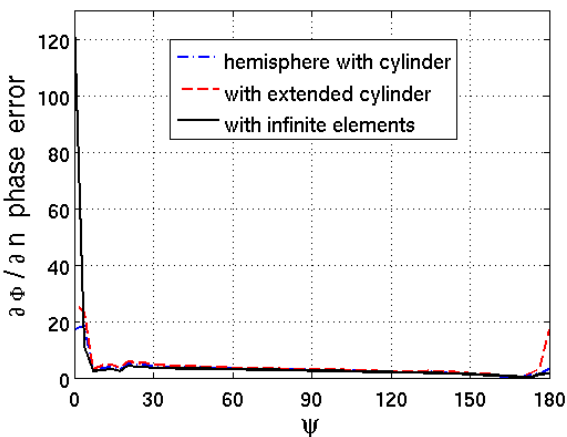


Figure 9. Solution differences for  $\partial\Phi/\partial n$  phase compared to hemisphere model.

### 3 CONCLUSIONS

Further improvement can be done by constructing a smooth connection between breast and chest instead of perpendicular ones and maybe by building two layer model where the second layer will correspond to a part of

chest. Except single points located on the hemisphere basis circumference there are no significant results deflection for extended models. If so it is to say that model with incorporated infinite elements offers the similar accuracy and almost 4 times shorter calculation times.

### 4 ACKNOWLEDGEMENTS

This work was partly supported by Polish Ministry of Science and Higher Education from funds for the years 2008-2009 as a research project No. N N519 1203 33 and N N510 3423 34

### 5 REFERENCES

- [1] Arridge S. R., Optical tomography in medical imaging, *Inverse Problems*, 1999, vol.15, No.2, pp.R41-R93
- [2] Arridge S. R., Schweiger M., The UCL optical tomography software system (TOAST). available at <http://www.medphys.ucl.ac.uk/~martins/toast/index.html>, 2004.
- [3] Beer G., Watson J. O., Infinite Boundary Elements, *International Journal for Numerical Methods in Engineering*, vol. 28, pp. 1233 - 1247, 1989.
- [4] Beer G., Watson J. O., Swoboda G., Three-dimensional analysis of tunnels using infinite boundary elements, *Computers and Geotechnics*, vol.3, pp. 37-58, 1987.
- [5] Bettess P., *Infinite Elements*, Penshaw Press, 1992
- [6] Sikora J., *Boundary Element Method for Impedance and Optical Tomography*, Oficyna Wydawnicza Politechniki Warszawskiej, Warsaw 2007.
- [7] Tarvainen T., *Computational Methods for Light Transport in Optical Tomography*, PhD Thesis, Department of Physics, University of Kuopio, 2006., [http://physics.uku.fi/~vilhunen/phdthesis\\_ttarvainen.pdf](http://physics.uku.fi/~vilhunen/phdthesis_ttarvainen.pdf)
- [8] Zacharopoulos A., Arridge S. R., Dorn O., Kolehmainen V., Sikora J., Three-dimensional reconstruction of shape and piecewise constant region values for optical tomography using spherical harmonic parametrization and a boundary element method, *Inverse Problems*, vol.22, pp.1-24, 2006.

Maciej Panczyk, M.Sc. Eng.  
 Computer Science Department  
 Lublin University of Technology  
 Nadbystrzycka 36B  
 20-618 Lublin , Poland  
 e-mail: maciej.panczyk@gmail.com

Prof. Jan Sikora, D.Sc. Ph.D.  
 Electronic Department  
 Lublin University of Technology  
 Nadbystrzycka 38A  
 20-618 Lublin , Poland  
 e-mail: sik59@wp.pl